Journal of Biomedical Optics

SPIEDigitalLibrary.org/jbo

Second harmonic generation signal in collagen fibers: role of polarization, numerical aperture, and wavelength

Oscar del Barco
Juan M. Bueno

SPIE

Second harmonic generation signal in collagen fibers: role of polarization, numerical aperture, and wavelength

Oscar del Barco and Juan M. Bueno
Universidad de Murcia, Laboratorio de Optica, Centro de Investigación en Optica y Nanofísica, Campus de Espinardo (Ed. 34), 30100 Murcia, Spain

Abstract. The spatial distribution of second harmonic generation (SHG) signal from collagen fibers for incident elliptical polarized light has been modeled. The beam was assumed to focus on a horizontal fiber through a microscope objective. For elliptical polarized states located along a vertical meridian of the Poincare sphere, the SHG intensity has been optimized in terms of the incident wavelength and the numerical aperture (NA) of the objective. Our results show that polarization modulates the SHG signal. Elliptical polarization can generate high signals (even greater than those corresponding to linear polarization) when combined with appropriate values of both incident wavelength and NA. On the other hand, the SHG intensity might also be identically zero for particular elliptical polarization states, a condition that depends exclusively on the ratio of hyperpolarizabilities of the collagen fibers. The highest forward-to-backward SHG signal distribution occurs along the propagating direction, depends on the incident wavelength, and reduces when NA increases. Furthermore, the direction of maximum SHG emission was found to be more sensitive to changes in the NA rather than variations in the incident wavelength. These findings could help to optimize the experimental conditions of multiphoton microscopes and to increase SHG signals from biological tissues containing collagen. [DOI: 10.1117/1.JBO.17.4.045005]

Keywords: second harmonic generation; collagen; nonlinear microscopy; polarization.

Paper 11308 received Jun. 20, 2011; revised manuscript received Feb. 17, 2012; accepted for publication Feb. 17, 2012; published online Apr. 19, 2012.

1 Introduction

During the last years there has been an increasing interest in the use of multiphoton microscopy for biomedical applications. In particular, second harmonic generation (SHG) imaging is a noninvasive technique that conserves energy, provides useful information on microscopic structures, and allows optical three-dimensional (3-D) sectioning and deep penetration.[1,2] Although, it is well known that SHG signal originates from noncentrosymmetric structures such as collagen,[1,3] this nonlinear process is also sensitive to local anisotropy,[4] distribution of molecular hyperpolarizabilities,[5] and phase-matching properties.[6] SHG is a coherent process involving phase-matching considerations whose emission is mainly directed rather than isotropic. SHG directionality depends on the distribution of induced dipoles within the focal volume where the nonlinear process takes place.[7] Since momentum conservation provides a preferred SHG signal in the forward direction (F-SHG) (i.e., along the incident direction of the laser beam), most nonlinear microscopes adopt this experimental configuration. Clinical applications involving SHG imaging of collagen structures in animals often require a backward collection geometry (B-SHG). Moreover, the structure of extracellular collagen plays an important role in cancerous processes (tumor development), aging and wound healing.[8] Several works have compared F-SHG and B-SHG imaging in different specimens containing collagen, such as endometrium tissue,[4] tendons,[9,10] corneal stroma,[11,12] skin,[6,13] and tumors,[14] among others. All these studies conclude that the SHG imaged structures strongly depend on the recording configurations of the microscope. On the other hand, theoretical works discussing the differences between F-SHG and B-SHG signals have also been reported.[10,15]

Linear polarized light has been shown to visualize different features of samples containing collagen, when imaged by means of SHG microscopy.[16–20] Whereas, some experiments and theoretical models were restricted to study the effects of incident linear polarized light on SHG imaging,[10,15,21] others have investigated the use of elliptical polarization to monitor molecular orientation[22] and to analyze the SHG signal from surfaces and films.[23,24] Some studies have also reported the effects of circular and elliptical polarization on the SHG intensity.[25,26] In particular, Schön et al.[26] showed that the dichroic mirrors used in the microscope collection optics can induce high levels of ellipticity in the incident beam, what leads to severe distortions in the polarization response. These distortions can be corrected by combining a half-wave plate and a quarter-wave plate.[25]

The aim of this work is to model and characterize the spatial distribution of SHG signal originated from collagen for focused elliptical polarized light. In Sec. 2 this theoretical model is developed. As a result, an analytical expression for the SHG intensity signal $I_{2\omega}$ as a function of the incident state of polarization, the fundamental wavelength λ_{ω}, and the numerical aperture (NA) of the microscope objective is derived. An extensively numerical analysis of $I_{2\omega}$ is described in Sec. 3, while Sec. 4 contains the discussion and the main conclusions of this work. Moreover, two appendixes with details on the calculation of the dipole moment induced by the incident electric field (Appendix A) as well as the total radiated SHG signal in the far field approximation (Appendix B) are also included.

Address all correspondence to: Juan M. Bueno, Universidad de Murcia, Laboratorio de Optica, Centro de Investigación en Optica y Nanofísica, Campus de Espinardo (Ed. 34), 30100 Murcia, Spain; E-mail: bueno@um.es

0091-3286/2012/$25.00 © 2012 SPIE

2 SHG Intensity Signal for Elliptically Polarized Light Focused on a Collagen Fiber

Let us consider a beam of elliptical polarized light with fundamental frequency ω propagating in the $\hat{z}$ direction (see Fig. 1) focusing through a microscope objective with numerical aperture NA $= n_\omega \sin\Theta$ on a collagen fiber lying along the $\hat{x}$ direction. Θ corresponds to the maximum angle at which the light rays enter the objective, while n_ω represents the index of refraction of collagen. The dependence of n_ω with the fundamental wavelength λ_ω of the incident light has been reported to be[27]

$$n_\omega(\lambda_\omega) = 1426 + \frac{19476}{\lambda_\omega^2} - \frac{1131066900}{\lambda_\omega^4}, \tag{1}$$

where λ_ω is expressed in nanometers. The perpendicular components of the elliptical polarized light $E_{\omega,x}$ and $E_{\omega,y}$ can be written as

$$E_{\omega,x}(x,y,z) = -i\,E_{\omega,x}^{(0)} \exp\left[-\left(\frac{x^2+y^2}{w_{xy}^2} + \frac{z^2}{w_z^2}\right)\right] \exp[i\xi k_\omega z], \tag{2}$$

$$E_{\omega,y}(x,y,z) = -i\,E_{\omega,y}^{(0)} \exp\left[-\left(\frac{x^2+y^2}{w_{xy}^2} + \frac{z^2}{w_z^2}\right)\right] \times \exp\left[i(\xi k_\omega z + \delta)\right], \tag{3}$$

where δ is the phase difference between these components, and $k_\omega = (2\pi n_\omega)/\lambda_\omega$ the wave number in a medium with index of refraction n_ω. ξ corresponds to the wave-vector reduction factor that characterizes the phase shift experienced by a Gaussian beam in the vicinity of a focal center.[15,28] For NAs lower than 1.2, ξ can be approximated by $\cos(\Theta/\sqrt{2})$. On the other hand, w_{xy} and w_z represent the $1/e$ radii of the focal ellipse in the lateral and axial directions, respectively[8,10,29]

$$w_{xy} = \frac{0.32\lambda_\omega}{n_\omega \sin\Theta} \qquad w_z = \frac{0.53\lambda_\omega}{n_\omega(1-\cos\Theta)}. \tag{4}$$

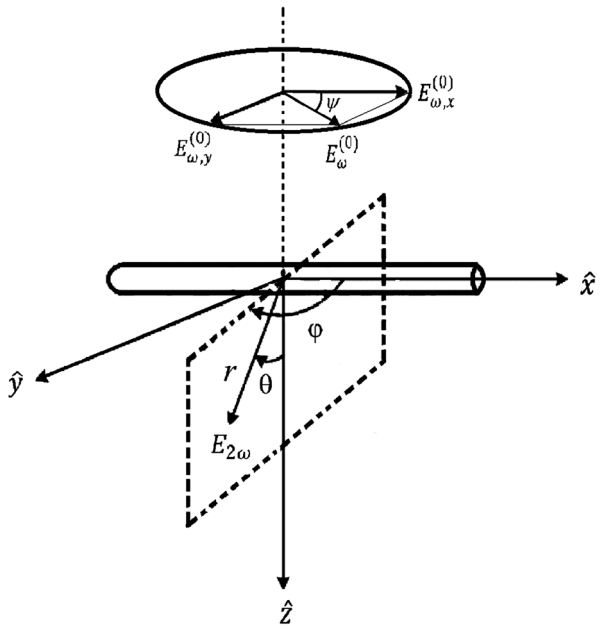

Fig. 1 A beam of elliptical polarized light with fundamental frequency ω, propagating in the $\hat{z}$ direction, focusing through a microscope objective with numerical aperture NA on a collagen fiber lying along the $\hat{x}$ direction.

As shown in Fig. 1, ψ symbolizes the ellipticity of the incident beam. For the sake of simplicity, the azimuthal angle of the ellipse of polarization has been chosen to be zero. This light conditions represent all the possible polarization states located along the null azimuth meridian on the Poincare sphere, what is consistent with sets of experimental polarization states provided by liquid-crystals.[30] This assumption will notably simplify our theoretical model since each component of the incident field $E_{\omega,x}$ and $E_{\omega,y}$ induces an SHG dipole moment along the collagen fiber ($\hat{x}$ direction). Appendix A explicitly shows that the dipole moments $\mu_{2\omega,x}^{(x)}$ and $\mu_{2\omega,x}^{(y)}$ induced by the electric fields $E_{\omega,x}$ and $E_{\omega,y}$ can , respectively be expressed as

$$\mu_{2\omega,x}^{(x)}(x,y,z) = \frac{1}{2}E_{\omega,x}^2\beta_{xxx}, \tag{5}$$

$$\mu_{2\omega,x}^{(y)}(x,y,z) = \frac{1}{2}E_{\omega,y}^2\beta_{xyy}, \tag{6}$$

where β_{xxx} and β_{xyy} correspond to the first hyperpolarizabilities contributing to the SHG field. Adding both quantities, the expression for the total SHG dipole moment will be

$$\mu_{2\omega}(x,y,z) = \mu_{2\omega,x}^{(x)}(x,y,z) + \mu_{2\omega,x}^{(y)}(x,y,z) = \frac{1}{2}(E_{\omega,x}^2\beta_{xxx} + E_{\omega,y}^2\beta_{xyy}). \tag{7}$$

This SHG dipole moment is directly related to the SHG far field $\vec{E}_{2\omega}$ radiated in the (θ,φ) direction[15,28,31,32]

$$\vec{E}_{2\omega}(\Psi) = \eta\vec{\mu}_{2\omega}\,\sin(\Psi)\exp[-i\vec{k}_{2\omega}\cdot\vec{r}]\hat{\Psi}, \tag{8}$$

where $\eta = \omega^2/\pi\epsilon_0 c^2$ and $\hat{\Psi}$ represents the angle between the $\hat{x}$ axis of the collagen fiber and the direction of emission $\vec{r}$ of the SHG field. ϵ_0 is the free-space permittivity, c the vacuum speed of light, and $k_{2\omega} = (2\pi n_{2\omega})/\lambda_{2\omega}$ the wave number for the SHG signal.

The total radiated SHG signal in the far field approximation is obtained by integration from all scatterers that have a dipole volume density defined by N_v[15] (see Appendix B)

$$E_{2\omega,x}(r,\theta,\varphi) = \frac{1}{2}\left[\left(\sqrt{\frac{\pi}{2}}\right)^3 w_{xy}^2 w_z\right] \times N_v\frac{\eta}{r}\left(\sin^2\theta\sin^2\varphi + \cos^2\theta\right)^{1/2} \times \exp\left[-\frac{k_{2\omega}^2}{8}(w_{xy}^2\,\sin^2\theta + w_z^2(\cos\theta - \xi')^2)\right] \times[(E_{\omega,x}^{(0)})^2\beta_{xxx} + (E_{\omega,y}^{(0)})^2\beta_{xyy}\exp[i2\delta]], \tag{9}$$

with $\xi' = \xi(n_\omega/n_{2\omega})$.

Therefore, the SHG intensity signal $I_{2\omega}$ can be written in terms of the electric field as

$$I_{2\omega}(r,\theta,\varphi)=\frac{1}{2}n_{2\omega}\epsilon_0 c|E_{2\omega,x}|^2$$
$$=\left[\frac{1}{8}n_{2\omega}\epsilon_0 c(N_v V)^2\right]\left(\frac{\eta}{r}\right)^2(\sin^2\theta\sin^2\varphi+\cos^2\theta)$$
$$\times\exp\left[-\frac{k_{2\omega}^2}{4}(w_{xy}^2\sin^2\theta+w_z^2(\cos\theta-\xi')^2)\right]$$
$$\times[(E_{\omega,x}^{(0)})^4\beta_{xxx}^2+(E_{\omega,y}^{(0)})^4\beta_{xyy}^2$$
$$+2(E_{\omega,x}^{(0)})^2(E_{\omega,y}^{(0)})^2\beta_{xxx}\beta_{xyy}\cos(2\delta)], \quad (10)$$

where V is the active SHG volume[31]

$$V=\left(\sqrt{\frac{\pi}{2}}\right)^3 w_{xy}^2 w_z. \quad (11)$$

From Fig. 1 the perpendicular components of the incident amplitude $E_\omega^{(0)}$ can easily be expressed as

$$E_{\omega,x}^{(0)}=E_\omega^{(0)}\cos\psi \qquad E_{\omega,y}^{(0)}=E_\omega^{(0)}\sin\psi, \quad (12)$$

then, Eq. (10) reduces to

$$I_{2\omega}(\psi,r,\theta,\varphi)$$
$$=\left[\frac{1}{8}n_{2\omega}\epsilon_0 c(N_v V)^2\right]\left(\frac{\eta}{r}\right)^2(\sin^2\theta\sin^2\varphi+\cos^2\theta)$$
$$\times\exp\left\{-\frac{k_{2\omega}^2}{4}[w_{xy}^2\sin^2\theta+w_z^2(\cos\theta-\xi')^2]\right\} \quad (13)$$
$$\times|E_\omega^{(0)}|^4\left[\cos^4\psi\beta_{xxx}^2+\sin^4\psi\beta_{xyy}^2\right.$$
$$\left.+\frac{1}{2}\sin^2(2\psi)\cos(2\delta)\beta_{xxx}\beta_{xyy}\right].$$

Equation (13) shows how the SHG signal explicitly depends on the ellipticity of the incident beam, ψ. Since the phase δ is equal to $\pm\pi/2$ for the elliptical polarized light here used (zero azimuth),[30] the final expression for the SHG intensity signal will be

$$I_{2\omega}(\psi,r,\theta,\varphi)$$
$$=\left[\frac{I_\omega^2}{2}\frac{n_{2\omega}}{n_\omega^2\epsilon_0 c}(N_v V)^2\right]\left(\frac{\eta}{r}\right)^2(\sin^2\theta\sin^2\varphi+\cos^2\theta)$$
$$\times\exp\left\{-\frac{k_{2\omega}^2}{4}[w_{xy}^2\sin^2\theta+w_z^2(\cos\theta-\xi')^2]\right\}$$
$$\times\left[\cos^4\psi\beta_{xxx}^2+\sin^4\psi\beta_{xyy}^2-\frac{1}{2}\sin^2(2\psi)\beta_{xxx}\beta_{xyy}\right], \quad (14)$$

where $I_\omega=(1/2)n_\omega\epsilon_0 c|E_\omega^{(0)}|^2$ corresponds to the intensity of the incident beam.

It can be noticed that the last term in Eq. (14) contains the polarization contribution to $I_{2\omega}$ via the ellipticity of the incident beam ψ. This factor must be taken into consideration for a complete description of the SHG intensity, as it will be shown in detail in the next section.

3 Analysis of the SHG Intensity Signal

Once our general expression of the SHG intensity signal $I_{2\omega}$ for elliptically polarized light has been obtained, a numerical analysis of this magnitude as a function of different parameters, such as the polarization state of the incident beam, the incident wavelength λ_ω, and the NA of the microscope objective will be carried out.

3.1 *Polarization Dependence of $I_{2\omega}$*

As above noticed, the analytical expression for $I_{2\omega}$ [Eq. (14)] includes a factor involving the polarization state of the incident light (elliptically polarized in general). Figure 2 shows the strong dependence of the SHG intensity on the ellipticity ψ of the incident light. Both F-SHG $I_{2\omega}^{(F)}$ (i.e., $-\pi/2<\theta<\pi/2$) and B-SHG $I_{2\omega}^{(B)}$ (i.e., $\pi/2<\theta<3\pi/2$) signals are plotted versus the polar coordinates (θ,φ) for four different polarization states (linear horizontal (H), right-handed elliptical with ellipticity 30 deg ($E_{R,30\ \mathrm{deg}}$), right-handed circular (C_R) and linear vertical (V). Since there exist several orders of magnitude between F-SHG and B-SHG, $I_{2\omega}^{(B)}$ has been plotted in logarithmic scale, for the sake of clarity. For these plots, λ_ω and NA were chosen to be 700 nm and 1.2, respectively. The refractive indexes corresponding to the SHG signal $n_{2\omega}$ and the incident light n_ω were computed by using Eq. (1) (1.509 and 1.461, respectively). The term $\{[I_\omega^2 n_{2\omega}(N_v V)^2]/(2n_\omega^2\epsilon_0 c)\}\times(\eta/r)^2$ was normalized to 1 for simplicity, and the selected value of the ratio of hyperpolarizabilities $\rho=\beta_{xxx}/\beta_{xyy}$ was 2.6 [ρ has been reported to range between -3 and 3 (Ref. 33)]. It can be observed that the maximum F-SHG intensity value occurs at the polar angle $\theta_{\max}=\arccos[\xi(n_\omega/n_{2\omega})]$ where the phase match condition $k_{2\omega}\cos\theta-2\xi k_\omega=0$ is satisfied.[10,15] For both F-SHG and B-SHG components, the SHG signal is maximum when the incident-polarized light is linear horizontal H (i.e., parallel to the collagen fibers' direction). Unlike expected, vertical polarization V does not minimize the SHG intensity. Right-handed circular polarized light (C_R) makes the SHG signal even smaller. This will be analyzed and discussed in the following paragraphs.

Let us now consider all the possible polarization states located along the meridian with null azimuth on the Poincare sphere. In this sense, Fig. 3(a) presents the maximum F-SHG intensity values $I_{2\omega,\max}^{(F)}$ as a function of the ellipticity of the incident beam ψ. The four polarization states described in Fig. 2 have also been labeled as well as the left-handed circular polarization state (C_L). In particular, when ψ equals 58.2 or 121.8 deg, the SHG intensity $I_{2\omega,\max}^{(F)}$ is identically zero, a fact that reveals the importance of the incident polarization state on the SHG signal. As expected, H polarized light yields a maximum $I_{2\omega,\max}^{(F)}$ value (see again Fig. 2). This SHG intensity is reduced when moving along the selected meridian on the Poincare sphere.[30] Figure 3(b) depicts the corresponding maximum values for F-SHG and B-SHG signals in logarithmic scale for direct comparison. It is observed that both curves have similar shapes with different orders of magnitude.

After analyzing the results shown in Fig. 3, a question arises: could $I_{2\omega}$ become identically zero by solely modifying the polarization state of the incident light? In order to answer this question, the roots of Eq. (14) were analytically computed. $I_{2\omega}$ vanishes for the following values of the ellipticity ψ_0

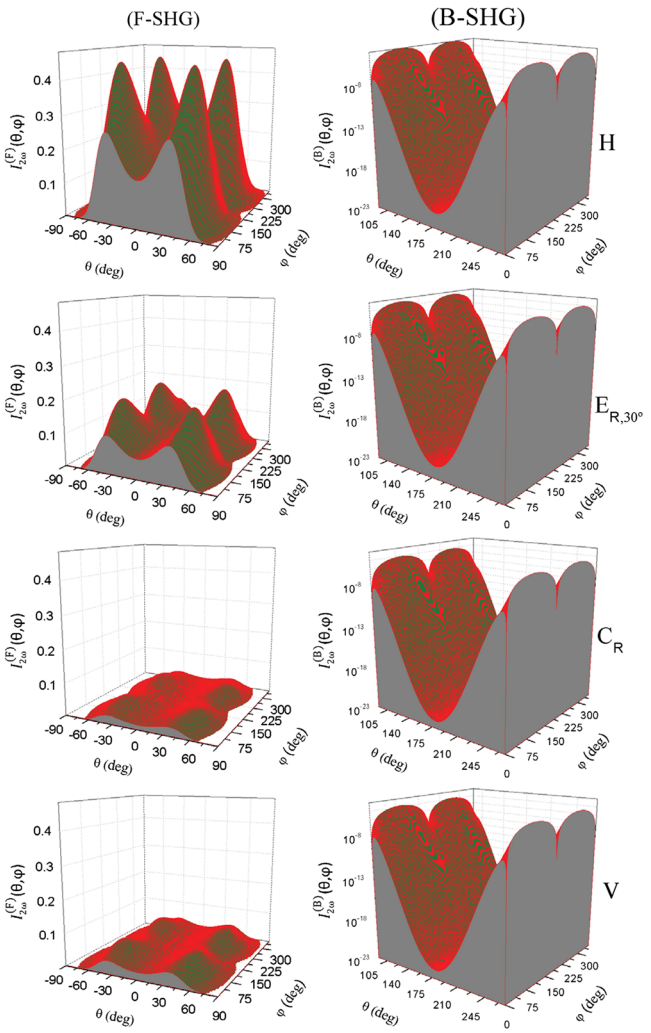

Fig. 2 F-SHG ($I^{(F)}_{2\omega}$, left column) and B-SHG ($I^{(B)}_{2\omega}$, right column) intensities versus polar coordinates (θ,φ) for four different polarization states (linear horizontal (H), right-handed elliptical with ellipticity 30 deg ($E_{R,30\ \mathrm{deg}}$), right-handed circular (C_R) and linear vertical (V). The fundamental wavelength λ_ω and the NA of the microscope objective have been chosen to be 700 nm and 1.2, respectively.

$$\psi_0 = \arccos(\pm 1/\sqrt{1+\rho}). \tag{15}$$

This expression depends exclusively on the ratio of hyperpolarizabilities ρ. Accordingly, Fig. 4 plots the values of ψ_0 as a function of ρ calculated via Eq. (15). It can be observed that, for a fixed value of ρ, there exist two ellipticity values (or equivalently, two polarization states in the meridian with null azimuth of the Poincare sphere) that vanish the SHG intensity. The existence of such polarization states is limited exclusively to values of $\rho > -1$, as can easily be deduced from simple inspection of Eq. (15).

3.2 *Effects of the Fundamental Wavelength and the Numerical Aperture on $I_{2\omega}$*

Results shown in Figs. 2–4 have been derived for the parameters $\lambda_\omega = 700$ nm and NA = 1.2. However, it is also interesting to investigate how the incident wavelength and the NA affect the SHG signal for different incident polarization states. In particular, Fig. 5(a) and 5(b) present two polar diagrams where the

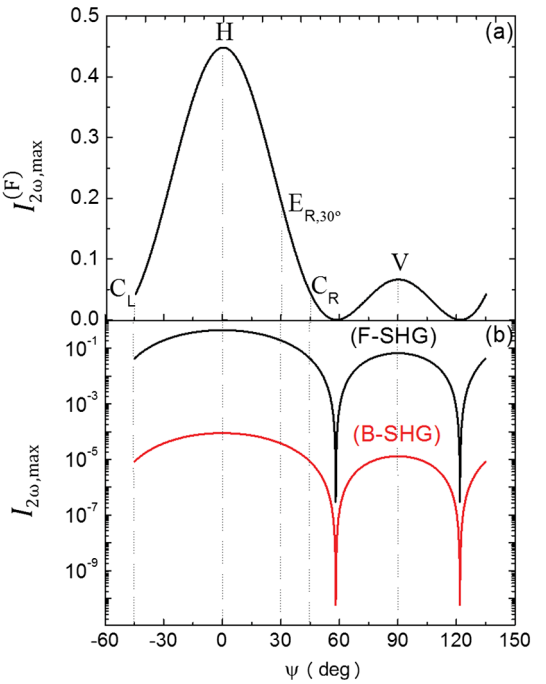

Fig. 3 (a) Maximum F-SHG intensity values $I^{(F)}_{2\omega,\mathrm{max}}$ and (b) maximum F-SHG and B-SHG intensity signals as a function of the ellipticity of the incident light ψ. Logarithmic scale has been used in Fig. 3(b) for a better comparison. C_L indicates left-handed circular polarized light.

B-SHG signal has been plotted as a function of 2ψ for different values of the λ_ω and NA, respectively. For a better comparison, the curves have been normalized to the maximum B-SHG intensity value ($\lambda_\omega = 1000$ nm and NA = 1.2 for the present case). As expected, for fixed values of the wavelength and the NA, the maximum B-SHG intensity occurs for horizontal polarized light H (what agrees with Figs. 2 and 3). However, for a chosen NA value, $I^{(B)}_{2\omega}$ increases with λ_ω, as shown in Fig. 5(a). That is, the maximum B-SHG intensity value will strongly depend on the incident wavelength value. As an example, an elliptical polarized light with $2\psi = 15°$ and $\lambda_\omega = 850$ nm focusing on a microscope objective with NA = 1.2, will generate a B-SHG signal 1.4 times larger than the signal produced by a horizontal polarized light with $\lambda_\omega = 700$ nm. From Fig. 5(b), the elliptical

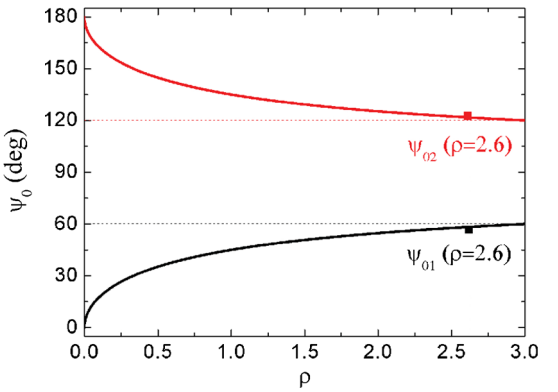

Fig. 4 Ellipticity values ψ_0 versus the ratio of hyperpolarizabilities ρ calculated via Eq. (15). For a fixed ρ there exist two possible values of ψ_0, which correspond to two different states along the meridian of the Poincare sphere with azimuth zero.

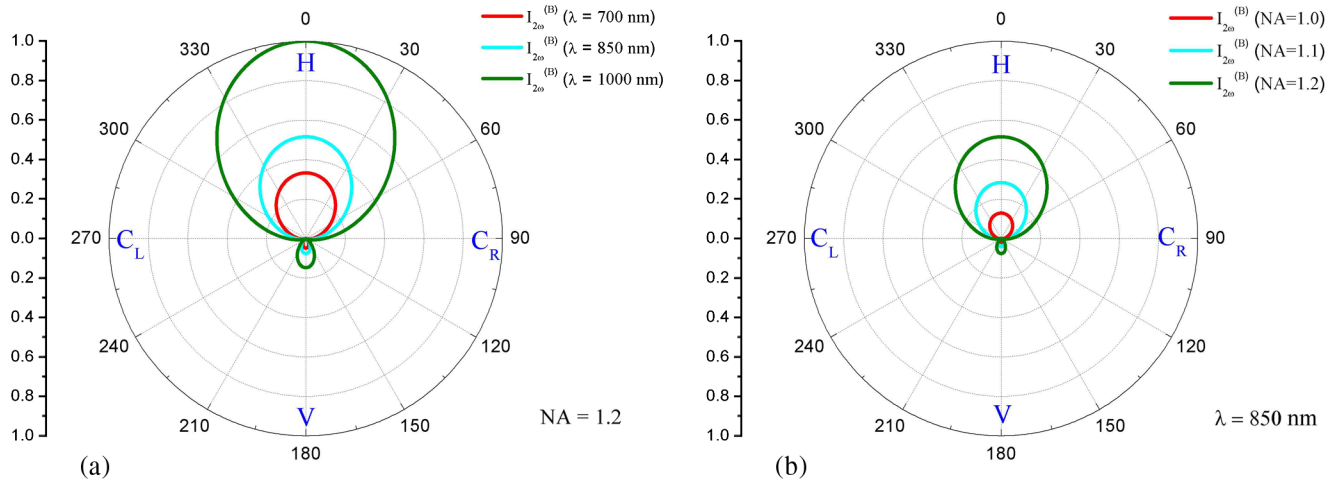

Fig. 5 B-SHG intensity $I^{(B)}_{2\omega,\max}$ as a function of 2ψ for different values of (a) the incident wavelength λ_ω (700, 850, and 1000 nm) and (b) the numerical aperture NA (1.0, 1.1, and 1.2). The results have been normalized to the maximum value of the B-SHG intensity ($\lambda_\omega = 1000$ nm and NA = 1.2, in our case) for a better comparison.

polarized light above cited will also generate a B-SHG signal 3.4 times larger than the corresponding H polarized light with an NA of 1.0. As a direct consequence, optimized values of the B-SHG signal can be achieved by using elliptical light combined with appropriate values of NA and λ_ω. Similar results have been found for the F-SHG intensity signal (not included in this work) so, these conclusions can also be extended to this SHG collection geometry.

On the other hand, from Eq. (14) it can easily be noticed that the F/B SHG ratio $I^{(F)}_{2\omega}/I^{(B)}_{2\omega}$ does not depend on the polarization state of the incident light (the last term cancels out). So, the effects of the incident wavelength λ_ω (i.e., chromatic dispersion) on the F/B SHG ratio have been investigated. Figure 6 shows the spatial distribution (expressed in polar coordinates (θ, φ)) of the F/B ratio for three different λ_ω values. For this plot, NA and ρ were chosen to be 1.2 and 2.6, respectively. It can be observed that the maximum F/B SHG ratio occurs along the propagating direction $\hat{z}$, that is, for $\theta = 0$. Moreover, the comparison of the F/B SHG spatial distributions for different λ_ω shows an increase of several orders of magnitude for higher values of λ_ω.

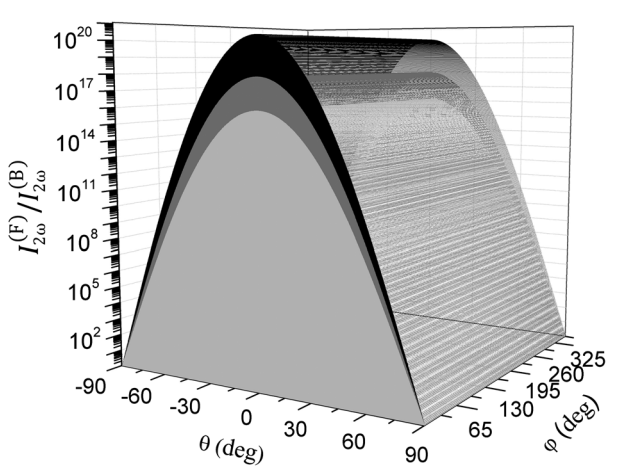

Fig. 6 F/B SHG intensity ratio $I^{(F)}_{2\omega}/I^{(B)}_{2\omega}$ versus the polar coordinates (θ, φ) for three different values of the fundamental wavelength λ_ω (grey: 700 nm, dark grey: 850 nm, and black: 1000 nm).

The effects of the NA on the F/B SHG ratio are presented in Fig. 7. The plot represents the $I^{(F)}_{2\omega}/I^{(B)}_{2\omega}$ spatial distribution for three different NA values. In this case, $\lambda_\omega = 850$ nm and $\rho = 2.6$. It can be observed that the NA of the microscope objective plays a fundamental role in the detected SHG signal. In particular, as the NA increases the spatial distribution spreads, and the F/B SHG ratio (which is always maximum along the direction of light propagation) decreases several orders of magnitude.

It is also worth while to study how the angle of maximum SHG intensity $\theta_{\max} = \arccos[\xi(n_\omega/n_{2\omega})]$ (which is independent on the ratio of hyperpolarizabilities ρ) depends on both λ_ω and NA. In this sense, Fig. 8(a) plots the polar angle $\theta_{\max}$ as a function of the NA for $\lambda_\omega = 850$ nm. These results show that, although $\theta_{\max}$ occurs always at forward propagation angles (i.e., $-\pi/2 < \theta < \pi/2$), it separates from the propagating direction $\hat{z}$ as the NA increases. In Fig. 8(b) this polar angle is represented versus the incident wavelength for NA = 1.2. We can conclude that the influence of the NA is stronger than the dispersion effects due to changes in the fundamental wavelength λ_ω. In particular, for the conditions here considered, when NA varied from 0.9 to 1.2, the angle of maximum SHG intensity $\theta_{\max}$ increased 65%. However this angle only increased 4% when λ_ω moved from 700 to 1000 nm.

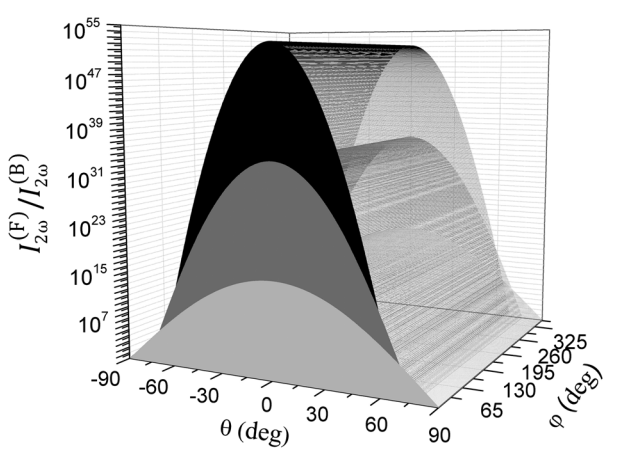

Fig. 7 Spatial distribution of the F/B SHG intensity ratio for different numerical aperture values (grey: 1.2, dark grey: 1.1, and black: 1.0).

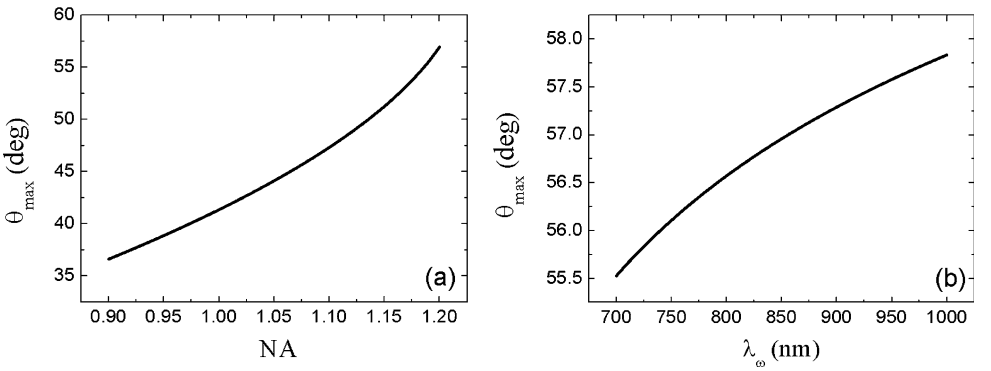

Fig. 8 Angle of maximum SHG intensity signal θ_{max} versus (a) the numerical aperture NA ($\lambda_\omega = 850$ nm) and (b) the incident wavelength λ_ω (NA = 1.2).

4 Discussion and Conclusions

A theoretical model to calculate the spatial distribution of $I_{2\omega}$ in collagen fibers for focused elliptical polarized light has been developed. A general expression involving the polar coordinates (θ, φ), the incident wavelength λ_ω, the NA of the microscope objective, and the ellipticity of the incident beam ψ has been obtained. For the sake of simplicity, collagen fibers were considered lying along the $\hat{x}$ direction. Under this assumption the spatial distribution was found to be anisotropic (see Fig. 2) for both F-SHG and B-SHG signals, although, the modulation of this anisotropy strongly depended on the incident polarization state. For fixed values of λ_ω and NA, the SHG signal presented maximum values for H linear polarized light (i.e., parallel to the direction of the collagen fibers) as shown in Figs. 2 and 3. This result is consistent with previously published work on SHG intensity signal for linear polarized light.[15] Unlike expected, vertical polarization does not minimize the SHG intensity, since C_R light makes this magnitude even smaller (see Fig. 3). However, $I_{2\omega}$ might also be identically zero for particular values of the ellipticity ψ_0 of the incident polarized light [see Eq. (15)]. This occurs when $\psi_0 = \arccos(\pm 1/\sqrt{1+\rho})$, a condition that depends exclusively on the ratio of hyperpolarizabilities ρ (Fig. 4). This fact must be taken into account when optimizing the SHG signal originated from a particular collagen sample. Incident polarization states must be "far away" from those verifying this condition. The effect of λ_ω and the NA of the microscope objective on the SHG intensity, besides its dependence on the incident polarization state, has also been investigated in detail. In general, for a fixed polarization state, the higher the values of the incident wavelength and the NA, the higher the SHG signal. Moreover, elliptical polarized light can produce SHG signals higher than those corresponding to H polarization when combined with appropriate values of both λ_ω and NA (see Fig. 5).

Multiphoton microscopy can be used in both F and B configurations. It has been experimentally shown that SHG microscopy images of tissues containing collagen are seen differently depending on the collection geometry used (forward or backward).[10,11,17] Having this into account, an in-depth analysis of the spatial distribution of the F/B SHG ratio has also been carried out. In particular, this distribution presents a maximum value along the propagating direction ($\theta = 0$) and significantly increases with the fundamental wavelength λ_ω (Fig. 6). This is an important fact that has previously been addressed by different authors.[12,34] On the other hand, as the NA increases, the spatial distribution spreads and the F/B SHG ratio decreases several orders of magnitude, as shown in Fig. 7. This corroborates the fundamental role played by the NA of the microscope objective in SHG detection.

Stoller et al. reported a study on the dependence of the F-SHG peak with the incident wavelength.[35] They obtained an increase of the normalized SHG peak signal with the NA, without taking into account the spatial resolved dependence. In a theoretical study, Chang and co-workers explored the combination effect of incident linear polarized light and the NA[15]. They reported that for NA < 0.4, the total SHG signal did not depend on polarization. However for higher values of NA there is a nonlinear dependence, which is particular for each polarization state. Since the present work explores the F/B SHG, the influence of the polarization state cancels out, as can easily deduced from Eq. (14).

Our numerical results have finally showed that independently of λ_ω and NA values, the angle of maximum SHG intensity θ_{max} always occurs at forward propagation angles. This will benefit the microscopes with forward experimental configurations. Furthermore, the influence of the NA on this angle is stronger than the dispersion effects due to changes in the fundamental wavelength (see Fig. 8).

SHG imaging of tissues composed of collagen is a topic of great interest in Biomedicine. As already reported, polarization dependence of the SHG signal can be used to increase the contrast in collagen SHG imaging,[16] to obtain information unreachable with intensity-based SHG microscopy[17,36] or to explore the sources of SHG signal within the specimen,[20,21] among others. The analysis of biological collagen-made structures with a noninvasive tool is important to understand and/or to monitor the effects of injury, healing process, surgery, pathologies, and thermal damages. The results reported here provide detailed information on how polarization can be used to optimize the SHG signal. Moreover, the analysis of the effects of both NA and incident wavelength might also be used to maximize the signal recorded with a multiphoton microscope. In particular, the implementation of these findings into SHG imaging devices would help to reduce the power of the incident laser beam in order to minimize photodamage, which is an issue in experiments with both *ex-vivo* and living tissues.

Appendix A: Dipole Moment Induced by the Incident Electric Field

In the particular case of a linear polarized beam at an angle α with respect to the collagen fiber ($\hat{x}$ direction), the SHG dipole moment can be written as[15]

$$\vec{\mu}_{2\omega}(x,y,z) = \frac{1}{2}\vec{E}^2_{\omega}(x,y,z) \times \begin{pmatrix} \beta_{xxx}\cos^2\alpha + \beta_{xyy}\sin^2\alpha \\ \beta_{xyy}\ \sin\ 2\alpha \\ 0 \end{pmatrix}. \tag{16}$$

Taking into account that the component $E_{\omega,x}$ of the incident field is linear polarized with $\alpha = 0$, Eq. (16) yields

$$\vec{\mu}^{(x)}_{2\omega}(x,y,z) = \frac{1}{2}\vec{E}^2_{\omega,x}(x,y,z) \times \begin{pmatrix} \beta_{xxx} \\ 0 \\ 0 \end{pmatrix}. \tag{17}$$

This expression reveals the absence of SHG dipole components in $\hat{y}$ and $\hat{z}$ directions. For this reason, the vectorial character of $\vec{\mu}^{(x)}_{2\omega}$ and $\vec{E}_{\omega,x}$ can be omitted and the SHG dipole moment induced by the electric field $E_{\omega,x}$ can be written as [see Eq. (5)]

$$\mu^{(x)}_{2\omega}(x,y,z) = \frac{1}{2}E^2_{\omega,x}(x,y,z)\beta_{xxx}. \tag{18}$$

Equivalently, the component of the incident field $E_{\omega,y}$ is also linear polarized with $\alpha = \pi/2$, so Eq. (16) turns into

$$\vec{\mu}^{(y)}_{2\omega}(x,y,z) = \frac{1}{2}\vec{E}^2_{\omega,y}(x,y,z) \times \begin{pmatrix} \beta_{xyy} \\ 0 \\ 0 \end{pmatrix}, \tag{19}$$

and the SHG dipole moment induced by $E_{\omega,y}$ can be expressed as [see Eq. (6)]

$$\mu^{(y)}_{2\omega}(x,y,z) = \frac{1}{2}E^2_{\omega,y}(x,y,z)\beta_{xyy}. \tag{20}$$

Appendix B: Total Radiated SHG Signal in the Far Field Approximation

The SHG far field is given by Eq. (8)

$$\vec{E}_{2\omega}(\Psi) = \eta\vec{\mu}_{2\omega}\ \sin(\Psi)\exp[-i\vec{k}_{2\omega}\cdot\vec{r}]\hat{\Psi}, \tag{21}$$

where, as mentioned, $\eta = \omega^2/\pi\epsilon_0 c^2$, Ψ represents the angle between the $\hat{x}$ axis and the emission direction $\vec{r}$ of the SHG field and $\sin(\Psi) = (\sin^2\theta\sin^2\varphi + \cos^2\theta)^{1/2}$. The total radiated SHG signal in the far field related to the SHG dipole moment $\mu^{(x)}_{2\omega}$ is the integrated one from all scatterers that have the dipole volume density defined by N_v. In polar coordinates, $E^{(x)}_{2\omega,x}(\theta,\varphi)$ can be expressed as[15]

$$\begin{aligned} E^{(x)}_{2\omega,x}(\theta,\varphi) = {} & \frac{\eta N_v}{r}(\sin^2\theta\sin^2\varphi + \cos^2\theta)^{1/2} \\ & \times \iiint \mathrm{d}x\mathrm{d}y\mathrm{d}z\,\frac{1}{2}(E^{(0)}_{\omega,x})^2\beta_{xxx} \\ & \times \exp\left(-2\frac{x^2+y^2}{w^2_{xy}} - 2\frac{z^2}{w^2_z} + 2i\xi k_\omega z\right) \\ & \times \exp[-ik_{2\omega}(z\cos\theta + y\sin\theta\sin\varphi \\ & + x\sin\theta\cos\varphi)], \end{aligned} \tag{22}$$

where Eq. (2) has been used for the calculation of the incident electric field $E_{\omega,x}$. Upon integration of Eq. (22) in x, y, and z directions from negative infinite to positive infinite, the total radiated SHG signal $E^{(x)}_{2\omega,x}$, is given by[15]

$$\begin{aligned} E^{(x)}_{2\omega,x}(\theta,\varphi) = {} & \frac{1}{2}\left[\left(\sqrt{\frac{\pi}{2}}\right)^3 w^2_{xy}w_z\right]N_v\frac{\eta}{r}(\sin^2\theta\sin^2\varphi+\cos^2\theta)^{1/2} \\ & \times\exp\left[-\frac{k^2_{2\omega}}{8}(w^2_{xy}\sin^2\theta + w^2_z(\cos\theta-\xi')^2)\right] \\ & \times(E^{(0)}_{\omega,x})^2\beta_{xxx}, \end{aligned} \tag{23}$$

where $\xi' = \xi(n_\omega/n_{2\omega})$.

Similarly, via Eq. (3), the following expression for the total radiated SHG signal in the far field related to the SHG dipole moment $\mu^{(y)}_{2\omega}$ can be obtained

$$\begin{aligned} E^{(y)}_{2\omega,x}(\theta,\varphi) = {} & \frac{1}{2}\left[\left(\sqrt{\frac{\pi}{2}}\right)^3 w^2_{xy}w_z\right]N_v\frac{\eta}{r}(\sin^2\theta\sin^2\varphi+\cos^2\theta)^{1/2} \\ & \times\exp\left[-\frac{k^2_{2\omega}}{8}(w^2_{xy}\sin^2\theta + w^2_z(\cos\theta-\xi')^2)\right] \\ & \times(E^{(0)}_{\omega,y})^2\beta_{xyy}\exp[i2\delta]. \end{aligned} \tag{24}$$

Finally, the expression for the total SHG signal $E_{2\omega,x}$ is obtained by adding Eq. (23) and (24)

$$\begin{aligned} E_{2\omega,x}(\theta,\varphi) = {} & \frac{1}{2}\left[\left(\sqrt{\frac{\pi}{2}}\right)^3 w^2_{xy}w_z\right]N_v\frac{\eta}{r}(\sin^2\theta\sin^2\varphi+\cos^2\theta)^{1/2} \\ & \times\exp\left[-\frac{k^2_{2\omega}}{8}(w^2_{xy}\sin^2\theta + w^2_z(\cos\theta-\xi')^2)\right] \\ & \times[(E^{(0)}_{\omega,x})^2\beta_{xxx} + (E^{(0)}_{\omega,y})^2\beta_{xyy}\exp[i2\delta]]. \end{aligned} \tag{25}$$

Acknowledgments

This work has been supported by "Ministerio de Ciencia e Innovación," Spain (Grants FIS2010-14926 and CONSOLIDER-INGENIO 2010, CSD2007-00033 SAUUL); Fundación Séneca (Región de Murcia, Spain), Grant 4524/GERM/06.

References

1. Y. Guo et al., "Second-harmonic tomography of tissues," *Opt. Lett.* **22**(17), 1323–1325 (1997).
2. P. J. Campagnola et al., "High-resolution nonlinear optical imaging of live cells by second harmonic generation," *Biophys. J.* **77**(6), 3341–3349 (1999).
3. S. Fine and W. P. Hansen, "Optical second harmonic generation in biological systems," *Appl. Opt.* **10**(10), 2350–2353 (1971).
4. G. Cox et al., "3-D imaging of collagen using second harmonic generation," *J. Struct. Biol.* **141**(1), 53–62 (2003).
5. I. Freund and M. Deutsch, "Second-harmonic microscopy of biological tissue," *Opt. Lett.* **11**(2), 94–96 (1986).
6. R. LaComb et al., "Phase matching considerations in second harmonic generation from tissues: effects on emission directionality, conversion efficiency and observed morphology," *Opt. Commun.* **281**(7), 1823–1832 (2008).
7. P. Stoller et al., "Quantitative second-harmonic generation microscopy in collagen," *Appl. Opt.* **42**(25), 5209–5219 (2003).
8. W. R. Zipfel, R. M. Williams, and W. W. Webb, "Nonlinear magic: multiphoton microscopy in the biosciences," *Nat. Biotechnol.* **21**(11), 1369–1377 (2003).
9. W. R. Zipfel et al., "Live tissue intrinsic emission microscopy using multiphoton-excited native fluorescence and second harmonic generation," *Proc. Natl. Acad. Sci. U. S. A.* **100**(12), 7075–7080 (2003).

10. R. M. Williams, W. R. Zipfel, and W. W. Webb, "Interpreting second-harmonic generation images of collagen I fibrils," *Biophys. J.* **88**(2), 1377–1386 (2005).
11. M. Han, G. Giese, and J. Bille, "Second harmonic generation imaging of collagen fibrils in cornea and sclera," *Opt. Express* **13**(15), 5791–5797 (2005).
12. N. Morishige et al., "Noninvasive corneal stromal collagen imaging using two-photon-generated second-harmonic signals," *J. Cataract. Refract. Surg.* **32**(11), 1784–1791 (2006).
13. S.-W. Chu et al., "Thickness dependence of optical second harmonic generation in collagen fibrils," *Opt. Express* **15**(19), 12005–12010 (2007).
14. X. Han et al., "Second harmonic properties of tumor collagen: determining the structural relationship between reactive stroma and healthy stroma," *Opt. Express* **16**(3), 1846–1859 (2008).
15. Y. Chang et al., "Theoretical simulation study of lineraly polarized light on microscopic second-harmonic generation in collagen type I," *J. Biomed. Opt.* **14**(4), 044016 (2009).
16. P. Stoller, K. M. Reiser, and P. M. Celliers, "Polarization-modulated second harmonic generation in collagen," *Biophys. J.* **82**(6), 3330–3342 (2002).
17. A. T. Yeh et al., "Selective corneal imaging using combined second-harmonic generation and two-photon excited fluorescence," *Opt. Lett.* **27**(23), 2082–2084 (2002).
18. M. Both et al., "Second harmonic imaging of intrinsic signals in muscle fibers in situ," *J. Biomed. Opt.* **9**(5), 882–892 (2004).
19. F. Tiaho, G. Recher, and D. Rouède, "Estimation of helical angles of myosin and collagen by second harmonic generation imaging microscopy," *Opt. Express* **15**(19), 12286–12295 (2007).
20. S. Psilodimitrakopoulos et al., "Quantitative discrimination between endogenous SHG sources in mammalian tissue, based on their polarization response," *Opt. Express* **17**(12), 10168–10176 (2009).
21. I. Gusachenko, G. Latour, and M. C. Schanne-Klein, "Polarization-resolved second harmonic microscopy in anisotropic thick tissues," *Opt. Express* **18**(18), 19339–19352 (2010).
22. V. Le Floc'h et al., "Monitoring of orientation in molecular ensembles by polarization sensitive nonlinear microscopy," *J. Phys. Chem. B* **107**(45), 12403–12410 (2003).
23. R. M. Plocinik et al., "Modular ellipsometric approach for mining structural information from nonlinear optical polarization analysis," *Phys. Rev. B* **72**(12), 125409 (2005).
24. N. J. Begue et al., "Nonlinear optical stokes ellipsometry. 2. experimental demonstration," *J. Phys. Chem. C* **113**(23), 10166–10175 (2009).
25. C.-K. Chou et al., "Polarization ellipticity compensation in polarization second-harmonic generation microscopy without specimen rotation," *J. Biomed. Opt.* **13**(1), 014005 (2008).
26. P. Schön et al., "Polarization distortion effects in polarimetric two-photon microscopy," *Opt. Express* **16**(25), 20891–20901 (2008).
27. A. N. Bashkatov et al., "Estimation of wavelength dependence of refractive index of collagen fibers of scleral tissue," *Proc. SPIE* **4162**, 265–268 (2000).
28. L. Moreaux, O. Sandre, and J. Mertz, "Membrane imaging by second-harmonic generation microscopy," *J. Opt. Soc. Am. B* **17**(10), 1685–1694 (2000).
29. R. Richards and E. Wolf, "Electromagnetic diffraction in optical systems.2. structure of the image field in an aplanatic system," *Proc. R. Soc. Lond. A. Math. Phys. Sci.* **253**(1274), 358–379 (1959).
30. J. M. Bueno, "Polarimetry using liquid-crystal variable retarders: theory and calibration," *J. Opt. A: Pure Appl. Opt.* **2**(3), 216–222 (2000).
31. J. Mertz and L. Moreaux, "Second-harmonic generation by focused excitation of inhomogeneously distributed scatterers," *Opt. Commun.* **196**(1–6), 325–330 (2001).
32. E. Hecht, *Optics*, Higher Education Press, Beijing (2005).
33. C. Odin et al., "Orientation fields of nonlinear biological fibrils by second harmonic generation microscopy," *J. Microsc.* **229**(1), 32–38 (2008).
34. B. Vohnsen and P. Artal, "Second-harmonic microscopy of ex vivo porcine corneas," *J. Microsc.* **232**(1), 158–163 (2008).
35. P. Stoller et al., "Quantitative second-harmonic generation microscopy in collagen," *Appl. Opt.* **42**(25), 5209–5219 (2003).
36. H. Bao et al., "Second harmonic generation imaging via nonlinear endomicroscopy," *Opt. Express* **18**(2), 1255–1260 (2010).